

Supporting Information:

Peak splitting and bias fields in ferroelectric hafnia mediated by interface charge effects

Moritz Engl,^{*,†} Wassim Hamouda,[‡] Ines Häusler,[‡] Suzanne Lancaster,[†] Luca Carpentieri,[†] Thomas Mikolajick,^{†,¶} Catherine Dubourdieu,^{*,‡} and Stefan Slesazeck^{*,†}

[†]*NaMLab gGmbH, 01187 Dresden*

[‡]*Helmholtz-Zentrum Berlin für Materialien und Energie, 14109 Berlin*

[¶]*Chair of Nanoelectronics, TU Dresden, 01187 Dresden*

[§]*Freie Universität Berlin, Physical and Theoretical Chemistry, 14195 Berlin*

E-mail: moritz.engl@namlab.com; catherine.dubourdieu@helmholtz-berlin.de;
stefan.slesazeck@namlab.com

TEM image

The image extraction for the TEM cross section of the materials is shown in Fig. S1.

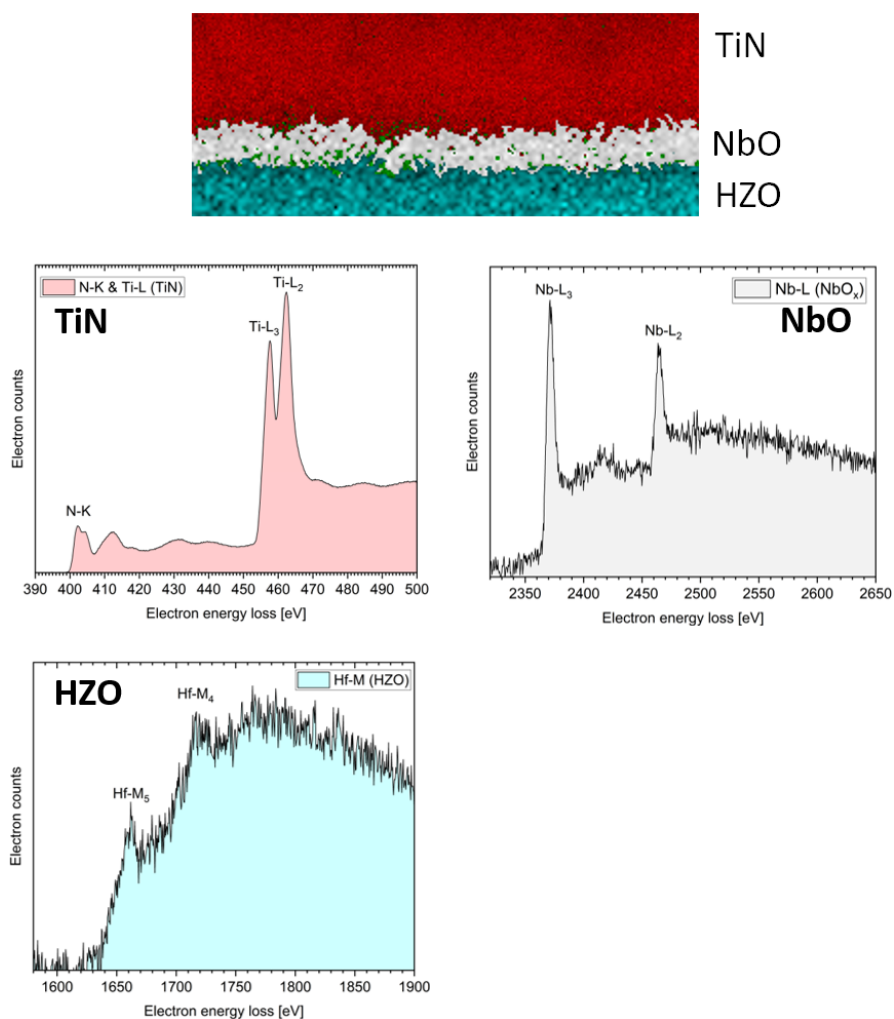


Figure S1: Overlay of EELS measurements for the different layers. Each color-dot in the cross section represents the occurrence of the signal for the specific material. For red dots the Ti signal, for grey the Nb signal and for blue the Hf signal is used.

Extraction of XPS data

The composition of NbO_x is calculated by analyzing the Nb 3d core level. The measurement results would indicate that 100% of the Nb is in the Nb^{5+} state, which means that all of the NbO_x is in the stoichiometry Nb_2O_5 . The deviation between fit and measured data, which can be caused by various physical mechanism as outlined in the manuscript, indicates that the extracted value might be incorrect and that the extraction of the Nb_2O_5 stoichiometry is beyond sensitivity.

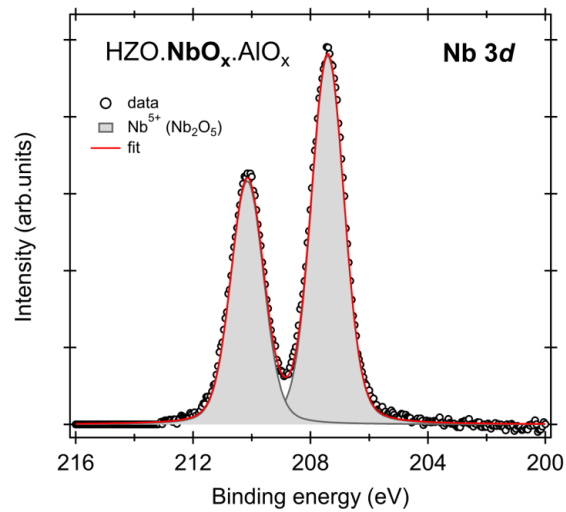


Figure S2: XPS measurement on the Hf 3d core level for the $\text{HZO.NbO}_x.\text{AlO}_x$ device. The red curve is the fit of the experimental data.

The composition of the aluminum oxide layer is calculated by analyzing the Al 2p core level. For the simulation it is assumed that only phases in the Al_2O_3 composition and pure metallic composition are present.

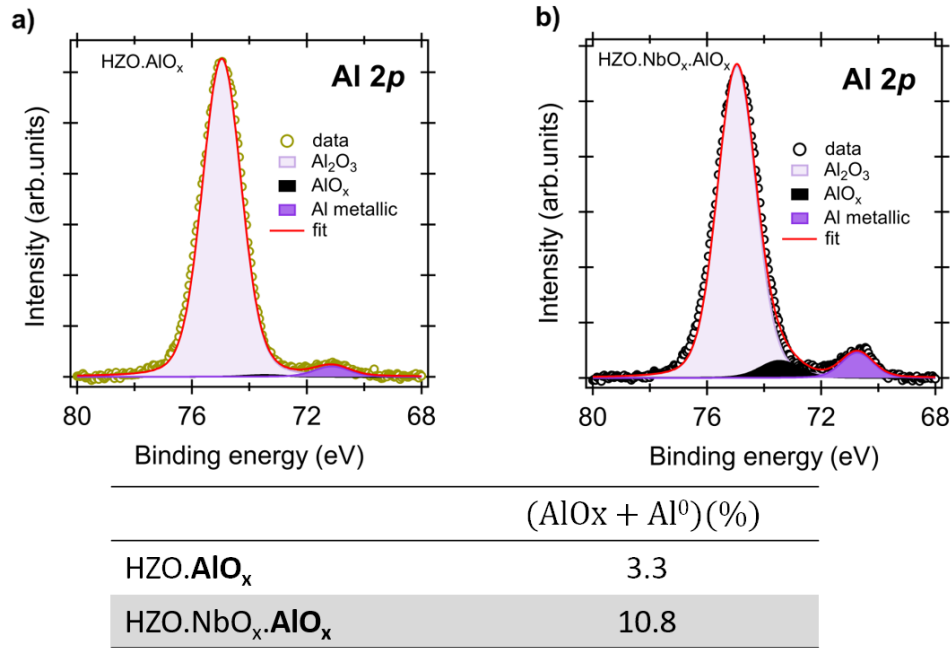


Figure S3: XPS measurement on the Al 2p core level for the HZO.AIO_x device in a) and for the HZO.NbO_x.AIO_x device in b). The red curve is the fit of the experimental data by assuming the presence of Al_2O_3 and metallic compositions in the aluminium oxide layer. The black curve is the difference between the fit and the measured data and represents the amount of Al not fitting in one of the two chemical compositions and thus representing substoichiometric AlO_x . In the table below is the extracted peak intensity of metallic Al and AlO_x in relation the measured peak intensity of the Al 2p core level shown.

Electrical measurements on XPS samples

Electrical measurements performed on the devices for XPS measurements are shown in Fig. S4. The Pr is higher and the peak-splitting is reduced for the HZO.NbO_x.AlO_x sample in comparison to the HZO.AlO_x sample.

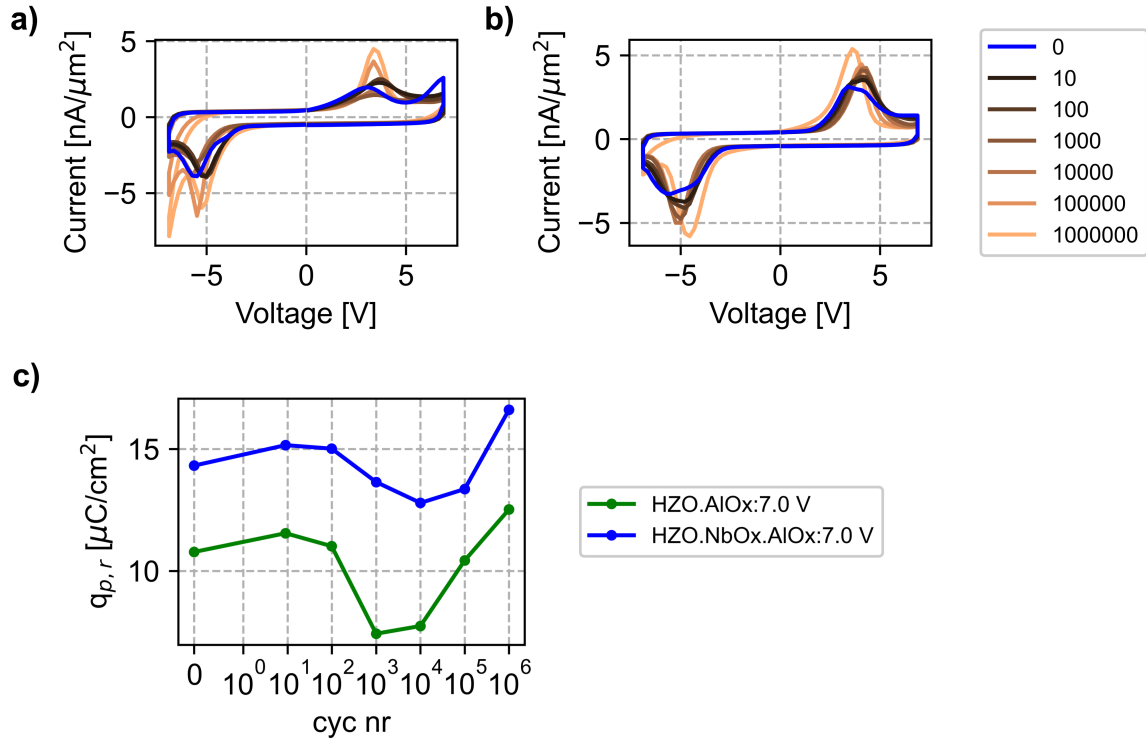


Figure S4: IV-curve development with cycling at 7 V for the HZO.AlO_x device in a) and HZO.NbO_x.AlO_x device in b). The charge of the P-U pulse with increasing number of cycles for 7 V is shown in c) for the HZO.AlO_x device in green and the HZO.NbO_x.AlO_x device in blue.

Measurement setup

The measurement setup used for all devices is shown in Fig. S5 a) with the cross section of a MFIM sample with HZO as ferroelectric and AlO_x as insulating layer. The used pulse sequence for electric characterization is depicted in Fig. S5 b).

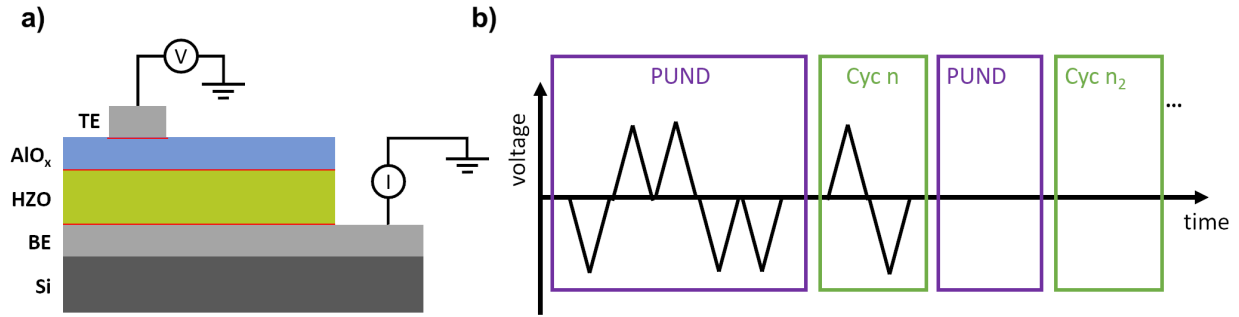


Figure S5: Measurement setup illustrated with a MFIM device in a) and used pulse sequence for IV-curve extraction in b). The frequency of the PUND measurement is 1 kHz and for the cycling 10 kHz. The amplitude for the measurement and cycling pulses is set to 3 V for devices without AlO_x layer and 7.5 V for devices with AlO_x layer.

Electrical Measurement data

Measurement of the polarizations with increasing amount of bipolar cycling for the samples used in TEM images and for electric characterization in Fig S6.

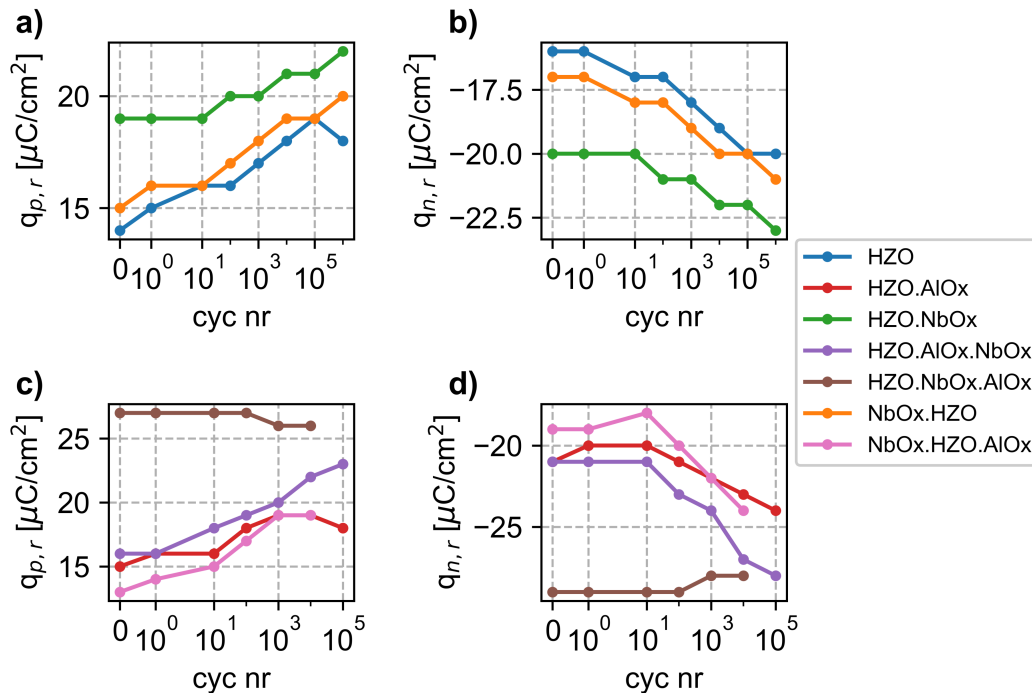


Figure S6: Measured remanent charge from the difference between P- and U- pulse vs number of cycling in a) and c) and from the difference between N- and D- pulse in b) and d). 3 V is used for the measurements of the samples without AlO_x and 7.5 V is used for the samples with AlO_x . Each color represents one sample type as shown in the legend.

The IV curves in Fig. S7 show that a stable IV behavior in the HZO.NbO_x.AlO_x sample over cycling is only achieved for cycling and measurement voltages that encompass the entire switching peak.

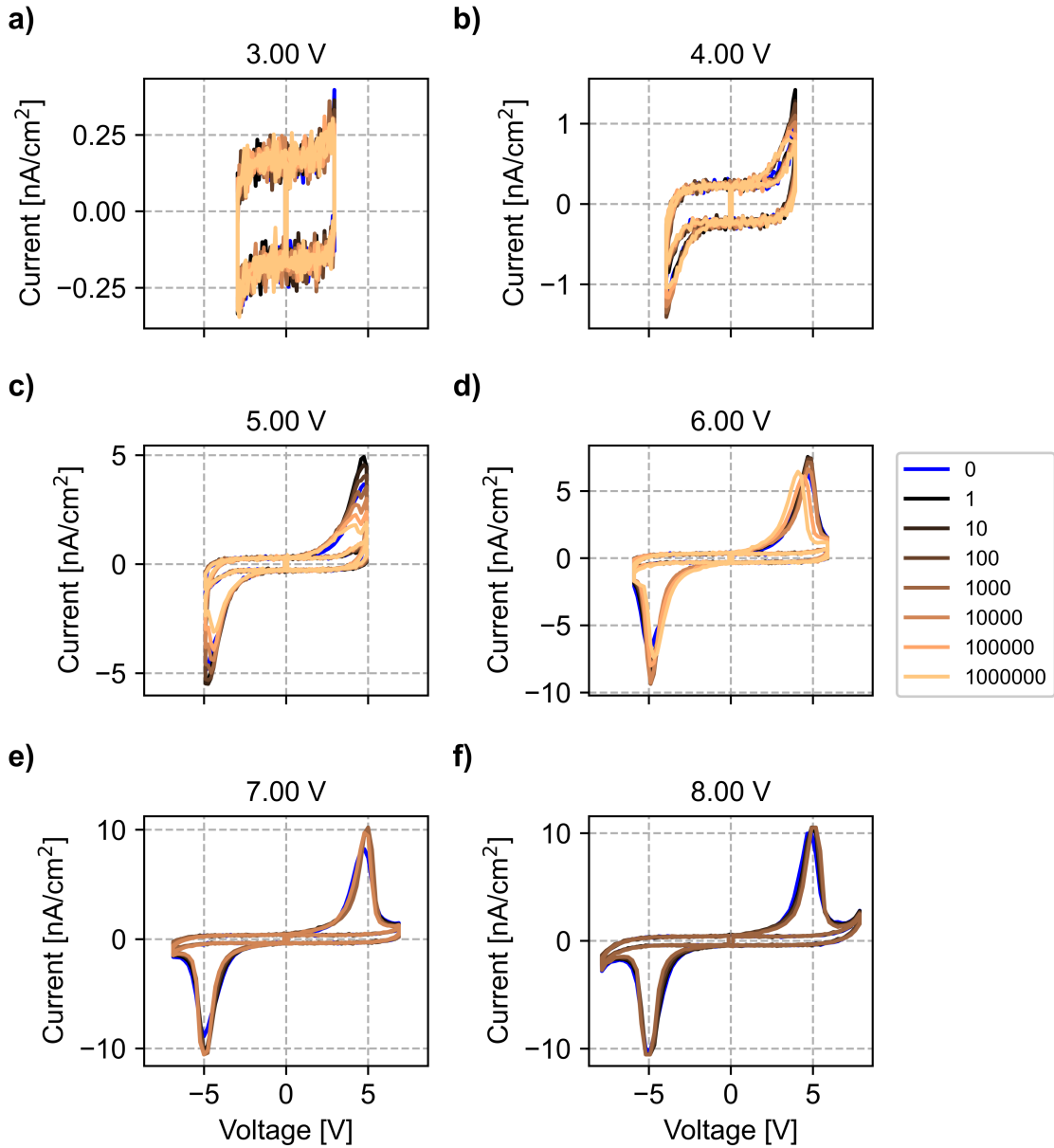


Figure S7: Measured IV curves of the HZO.NbO_x.AlO_x sample with increasing voltages from a) to f) as indicated by the subplot title. The voltage was used for cycling pulses and measurement pulses. The colors represent the number of cycles as shown in the legend.

Peak splitting and bias fields in ferroelectric hafnia mediated by interface charge effects

Moritz Engl,^{*,†} Wassim Hamouda,[‡] Ines Häusler,[‡] Suzanne Lancaster,[†] Luca Carpentieri,[†] Thomas Mikolajick,^{†,¶} Catherine Dubourdieu,^{*,‡} and Stefan Slesazek^{*,†}

[†]*NaMLab gGmbH, 01187 Dresden*

[‡]*Helmholtz-Zentrum Berlin für Materialien und Energie, 14109 Berlin*

[¶]*Chair of Nanoelectronics, TU Dresden, 01187 Dresden*

[§]*Freie Universität Berlin, Physical and Theoretical Chemistry, 14195 Berlin*

E-mail: moritz.engl@namlab.com; catherine.dubourdieu@helmholtz-berlin.de;
stefan.slesazek@namlab.com

Abstract

The pristine state of hafnium based ferroelectric devices exhibits various unwanted properties, such as imprint and peak splitting, which diminish with bipolar cycling. The incorporation of a niobium oxide layer at different positions in metal-ferroelectric-metal and metal-ferroelectric-insulator-metal stacks is used to modify the pristine state of the device. X-ray photoelectron spectroscopy and transmission electron microscopy measurements are used to investigate the influence of niobium oxide on the zirconium hafnium oxide layer. It is hypothesized that the charged vacancies generated by the introduced niobium oxide in the adjacent zirconium hafnium oxide layer result in an electric bias field that influences the pristine polarization state of the domains. A comparison of different stacks shows that peak splitting in the pristine state is most likely

related to the formation of opposing electric bias fields in upwards and downwards polarized domains. Furthermore, the incorporation of niobium oxide in the zirconium hafnium oxide/aluminum oxide capacitor stack in between the ferroelectric and insulating layer leads to a peak splitting free device without imprint, which could be explained by the increased influence of charge trapping near the zirconium hafnium oxide-/niobium oxide and niobium oxide-/aluminum oxide interfaces.

Introduction

Ferroelectric domains in hafnium oxide layers have two stable operation points with opposite polarization which arises from two energetically stable configurations of the ferroelectric orthorhombic phase.¹ The dynamic IV-curve, measured using the PUND method (Positive Up Negative Down),² exhibits the characteristic hysteresis with a specific remanent polarization. The initial state of ferroelectric capacitors based on hafnium oxide thin films usually exhibits multiple non ideal features in the IV-curve. These effects encompass for example an initial shift along the voltage axis of the hysteresis loop (imprint),^{3,4} peak splitting and therefore pinching^{4,5} of the hysteresis loop or wakeup (an increase of the remanent polarization with cycling⁵). The cycling instability of the hysteresis impedes the application of these films in actual devices and circuits, because either an initial cycling of the device before the actual operation is necessary or the changes during operation have to be considered in the design process of the circuit.

Recently it has been shown that a higher amount of orthorhombic phase and less peak splitting can be observed in metal-ferroelectric-metal (MFM) capacitors by using a TiO_x capping layer and a Nb_2O_5 capping layer between the zirconium doped hafnium oxide (HZO) layer and the TiN electrodes.^{6,7} It is assumed that TiO_x leads to a more favorable orientation of the grains in the HZO⁷ and that the introduced Nb_2O_5 layer acts as an oxygen source which reduces the amount of oxygen vacancies generated in the HZO.⁷

In Popovici et. al.⁷ the assumption that niobium oxide acts as an oxygen source is

supported by ab initio calculations and the lower electron affinity of Nb_2O_5 in comparison to HfO_2 and ZrO_2 , which indicates that the migration of oxygen ions from niobium oxide to the HZO is energetically more favorable. Nevertheless, pure niobium can be used in Pt-Nb- HfO_x -Pt structures as an oxygen exchange layer,⁸ which facilitates the formation of vacancies in the hafnium oxide layer. The use of Nb as an oxygen exchange layer indicates that the formation of niobium oxide phases may be energetically favourable and therefore non-stoichiometric niobium oxide may lead to the formation of oxygen vacancies in the HZO layer.

In this paper the initial state of metal-ferroelectric-metal (MFM) and metal-ferroelectric-insulator-metal (MFIM) is investigated with the introduction of a thin niobium oxide layer at different positions in the stacks. The investigations are based on two basic kinds of stacks, a MFM stack with HZO as the ferroelectric layer and a MFIM stack with HZO as the ferroelectric and aluminum oxide (AlO_x) as the insulating layer. The MFIM device with 4 nm AlO_x is used as a standard layer to observe negative capacitance (NC) as described in Engl. et. al.⁹

Furthermore, X-ray photoelectron spectroscopy (XPS) and transmission electron microscopy (TEM) measurements are performed to investigate the chemical interaction between HZO and niobium oxide.

Device structures

All devices were fabricated on p-doped silicon substrates. The bottom electrode was formed by sputtering 30 nm of W and 10 nm of TiN in high vacuum. Subsequently an ALD process at 280 degree with ozone as oxidant was used to deposit 10 nm of zirconium hafnium oxide (HZO) as the ferroelectric layer. For the MFIM samples 4 nm aluminium oxide (AlO_x) was deposited by ALD with water as oxidant. The top electrode consists of 10 nm TiN sputtered in high vacuum. An annealing step at 500 degrees Celsius for 20s in N_2 atmosphere was

used to crystallize the HZO after the deposition of the top TiN layer.

Subsequently 10 nm of Ti and 25 nm of Pt were evaporated and structured into rectangular dots in a lift-off process. The top TiN layer was etched by reactive ion etching with the use of the already structured Pt dots as etching masks. For the bottom electrode contact an additional lithography step was used followed by reactive ion etching of the ferroelectric/dielectric layer stack stopping on the tungsten electrode. The 1 nm thick niobium oxide (NbO_x) layer inserted in the different stacks was sputter deposited in high vacuum. The thickness of oxygen scavenging layers has been shown to be critical in either enhancing or degrading the ferroelectric properties,¹⁰ and layers around 1 nm are expected to be optimal for enhancing ferroelectricity, which may be dependent on the oxygen scavenging material.

The electrical properties of the device are influenced by the adjacent layers of the HZO.^{11,12} The induced tensile stress during the annealing¹² based on the difference in thermal expansion coefficients of the layers as well as the formation of interfaces¹¹ like titanium nitride oxide at the HZO-TiN interfaces impact the resulting distribution of phases in the HZO after the thermal anneal. It is assumed that an oxidation process^{11,13} during the anneal is responsible for the interfacial layer(s) generation by scavenging partially the necessary oxygen from the HZO layer and therefore generating oxygen vacancies within the HZO layer in proximity of the interface(s).¹¹⁻¹⁵ Considering the process flow of a MFM device with TiN as top and bottom electrode, the formation of an initial titanium nitride oxide layer is expected during the ALD process and the transfer process between the deposition tools which impedes the scavenging of oxygen during the annealing step,^{13,14} resulting in the formation of fewer vacancies at the bottom interface than at the top interface. In the case of a NbO_x layer below the HZO layer, the NbO_x layer is assumed to be more oxidized during the ALD deposition than the NbO_x in contact with the layer at top electrodes, similar to the investigations with tantalum oxide in Shin et al.¹⁶

The introduction of oxygen vacancies is associated with a higher orthorhombic phase fraction and thus a higher remanent polarization P_r , but is also considered to reduce device

endurance.¹¹ Furthermore, the redistribution and the additional formation of vacancies during cycling can be associated to the changes of device properties.^{4,5}

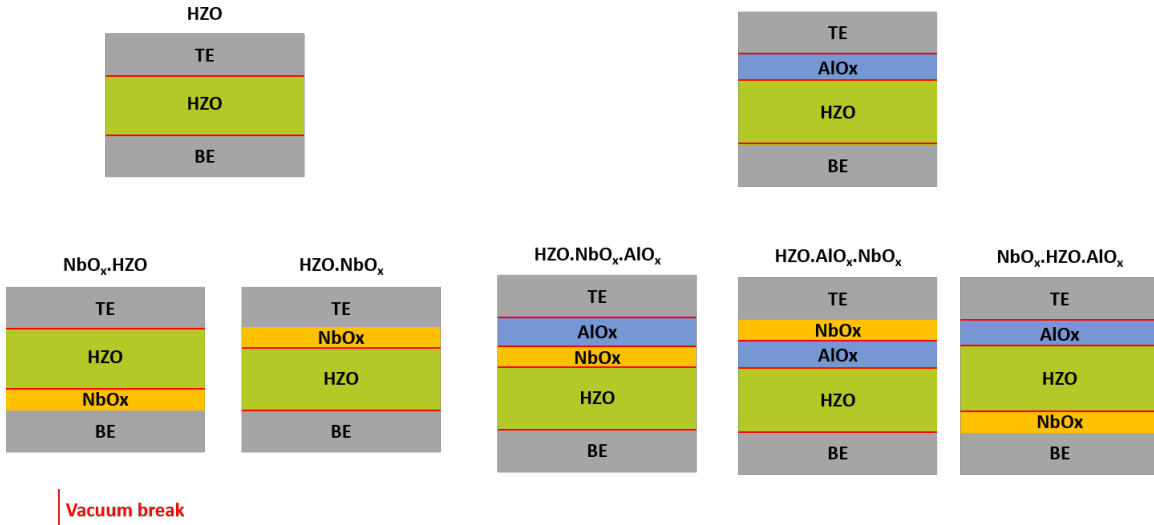


Figure 1: Schematic cross section of the investigated samples. TE is the top electrode and BE the bottom electrode. The name above each stack is used as a short name for the respective sample. A red line indicates that a vacuum brake during processing occurred.

Overall seven device types were manufactured for electrical measurements and analysis, as depicted in Fig. 1. The HAADF-STEM and EELS measurements in Fig. 2 show a comparable high roughness of the layers, as expected for polycrystalline layers, which has to be taken into account in the further analysis, since each measured signal in the EELS spectra is the superposition of several contributing atomic layers. The NbO_x.HZO sample (Fig. 3(a)) shows a broader distribution of the niobium signal and a higher oxygen signal near the NbO_x-/HZO interface compared to the ones in the HZO.NbO_x sample (Fig. 3(b)). The larger oxygen content is attributed to the exposure of the NbO_x layer to ozone in the first steps of the HZO growth. The broader Nb distribution is either caused by the diffusion of niobium in the HZO and/or TiN layer or it is a result of a difference in the roughness between the NbO_x layers in Fig. 3 a) and b). The HZO.NbO_x in Fig. 3 b) shows a higher nitrogen content in the NbO_x layer than the NbO_x.HZO sample in Fig. 3 a), which is attributed to the exposure of the NbO_x layer in the HZO.NbO_x sample to the nitrogen gas used in the reactive sputtering of TiN with a titanium target.

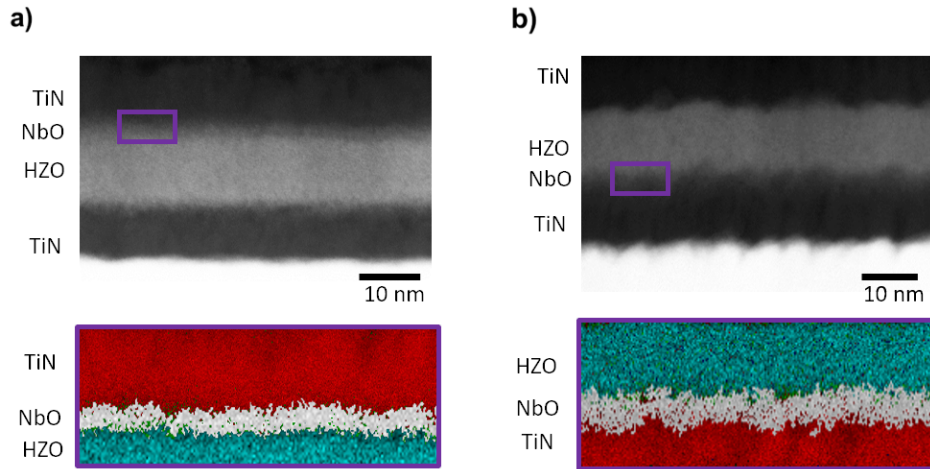


Figure 2: HAADF-STEM and EELS measurements of two samples HZO.NbO_x in a) and NbO_x.HZO in b). Each color in the magnified images in the bottom represents a signal from a specific element: red-N, grey-Nb, cyan-Hf and green-O. See Fig. S1 in the supplementals for more information.

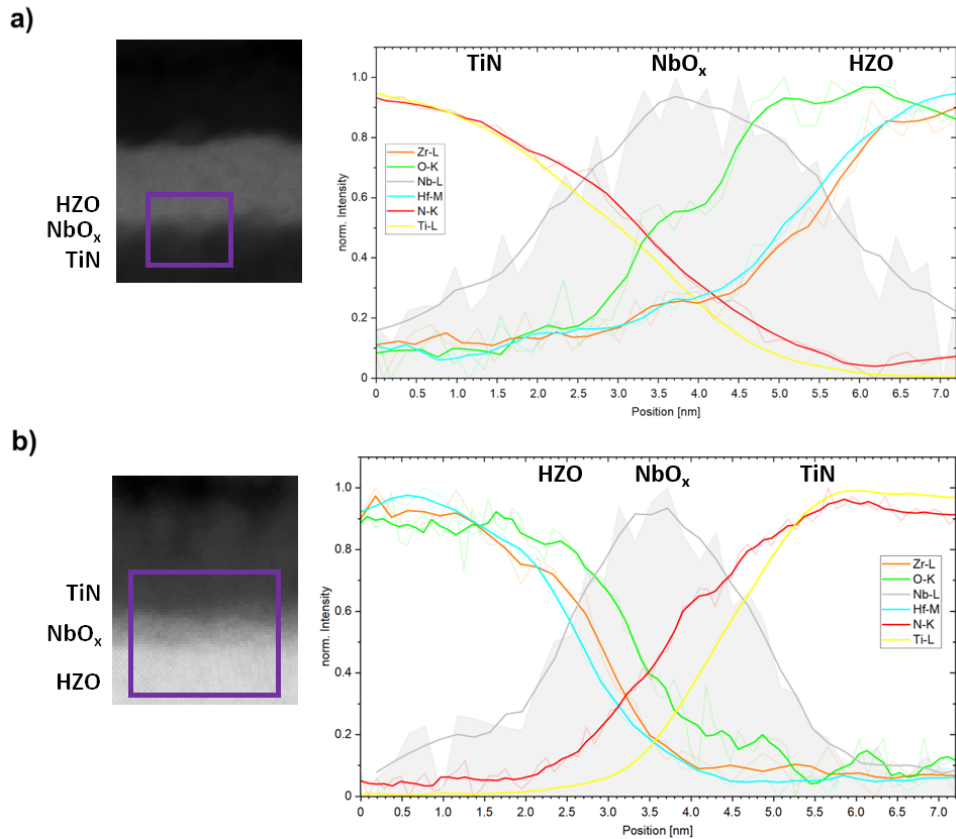


Figure 3: Elemental analysis for the TiN-NbO_x-HZO region of a NbO_x.HZO device in a) and the HZO-NbO_x-TiN region of a HZO.NbO_x device in b). The purple squares mark the region, where the analyses were carried out.

The XPS investigations required the manufacturing of different samples, since a measurement through the 20 nm thick Pt layer that defines the TE of the capacitor structure is not possible and the surface next to dots is most likely damaged by the dry etching of the TiN layer. For this experiment an alternative process flow was used. The deposition of TiN at the top electrode was skipped and the structuring of the Ti/Pt electrodes was done by a shadow mask. The contact to the bottom electrode for electric measurements was realized by electrically-broken capacitors which form an ohmic contact to the bottom electrode. The electrical properties of these samples are expected to be different from those annealed with a top TiN layer. Two samples, one HZO. AlO_x sample and one HZO. NbO_x . AlO_x sample, were manufactured. The HZO and AlO_x layers for the XPS experiments were deposited in the Oxford Instruments OpAL system.

The HZO and AlO_x layers for the electrical analysis and TEM measurements were deposited in the Scia Atol 200 tool from Scia Systems. The Opal system used HyALD and ZyALD as precursors, while the Scia system used TEMAHf as precursor. Despite having a similar HZO stoichiometry of $\text{Hf}_{0.4}\text{Zr}_{0.6}\text{O}_2$, the Scia samples exhibits more peak splitting in the pristine state, making it easier to study phenomena such as peak splitting in this particular experiment.

XPS investigations

XPS measurements were performed on HZO. AlO_x and HZO. NbO_x . AlO_x samples without top TiN layers. The concentration of oxygen vacancies, which are assumed to be positively charged, near the top of the HZO layer was calculated from the intensities $I_{\text{Hf}^{3+}}$ of the Hf^{3+} state and $I_{\text{Hf}^{4+}}$ of the Hf^{4+} state of the 4f orbital of the hafnium atoms, assuming that the formation of oxygen vacancies changes the charge state of the Hf atoms.

$$V_{\text{O}} = \frac{I_{\text{Hf}^{3+}}}{I_{\text{Hf}^{3+}} + I_{\text{Hf}^{4+}}} \cdot 0.5 \cdot 0.25 \quad (1)$$

The density of vacancies in the HZO.NbO_x sample is of $5.3 \times 10^{20} \text{ cm}^{-3}$, which is higher than the density of vacancies in the HZO.AlO_x sample of $0.7 \times 10^{20} \text{ cm}^{-3}$, as shown in Fig. 4.

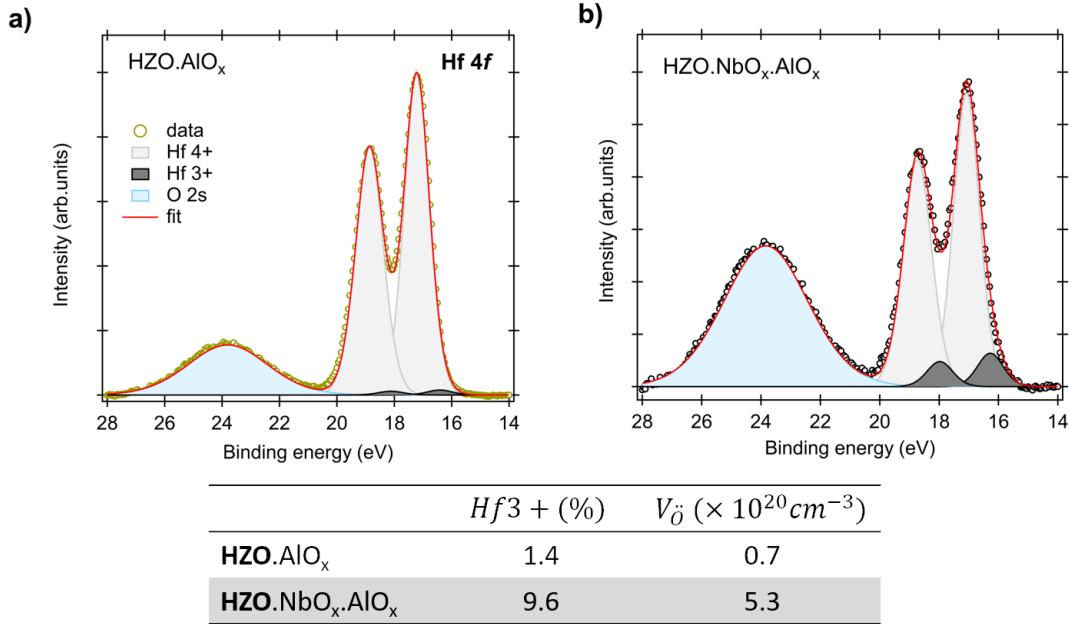


Figure 4: XPS measurements on the Hf 4f and O 2s core levels for the HZO.AlO_x device in a) and the HZO.NbO_x.AlO_x device in b). The red curve is the fit of the experimental data. In the table below the graphes, we give the intensity of the Hf3+ peak and the concentration of the oxygen vacancies calculated using equation 1.

The increase of oxygen vacancies in HZO by the insertion of the NbO_x layer on top indicates that NbO_x acts as an oxygen scavenger, thus increasing the amount of vacancies in the HZO layer. It should be noted that the NbO_x in this work is sputtered while the NbO_x in the literature^{6,7} is deposited by ALD, hence a difference in composition and defects is expected. The different behavior of the NbO_x is most likely related to a different stoichiometry after depositing the layer. The tendency to scavenge oxygen indicates that the NbO_x layer is not fully saturated with oxygen after deposition on top of HZO, and that oxygen is scavenged from neighboring layers to get closer to the most energetically favorable stoichiometry. According to theoretical calculations by Jacob et. al.,¹⁷ the introduction of defects in Nb₂O_{5-x} leads to a more stable composition than pure Nb₂O₅. An analysis of the NbO_x composition based on the 3d core level of Nb is beyond sensitivity, which is concluded from the deviation

between the measurement signal and the fit in Fig. S2 of the supplementary. The deviation could indicate a strong inter-diffusion of the materials, which can't be estimated due to the roughness of the layers, a high amount of defects in the NbO_x or the formation of substoichiometric oxide phases.

Furthermore, the analysis of the AlO_x layers in the $\text{HZO}.\text{AlO}_x$ and $\text{HZO}.\text{NbO}_x.\text{AlO}_x$ samples show, that the amount of stoichiometric Al_2O_3 decreases from 97 % in the $\text{HZO}.\text{AlO}_x$ sample to 89 % in the $\text{HZO}.\text{NbO}_x.\text{AlO}_x$ one. Therefore it can be assumed that NbO_x scavenges oxygen from AlO_x when in direct contact with it. A detailed analysis is shown in the supplementary Fig. S3.

An alternative explanation for the change of stoichiometric Al_2O_3 between the two samples is that the AlO_x layer scavenges oxygen from the HZO layer when in direct contact with it. The introduction of the NbO_x layer between the HZO and AlO_x acts as a barrier to this scavenging process. The presence of 7.6 times more charged vacancies in the $\text{HZO}.\text{NbO}_x.\text{AlO}_x$ sample than in the $\text{HZO}.\text{AlO}_x$ one (Fig. 4) indicates that NbO_x exhibits a greater tendency to scavenge oxygen compared to AlO_x . Therefore, the NbO_x layer most likely scavenges oxygen from the neighboring AlO_x layer and the neighboring HZO layer.

The electrical results for the two XPS samples are shown in the supplementary Fig. S4. They show similar trends to the other samples comprising the insertion of a NbO_x layer, which are discussed in the next section.

Electrical analysis of MFM with NbO_x incorporation

The electrical characterization was performed using a Keithley 4200A-SCS Parameter Analyzer in combination with a 4225 Pulse Measurement Unit (PMU) and 4225 Remote Preamplifier/Switch Modules (RPMs). For each measurement the bottom electrode was grounded and the pulses were applied to the top electrode of the device. The current was measured at the grounded bottom electrode to reduce the influences of parasitic capacitances from the

measurement setup. The ferroelectric properties were analyzed by PUND² measurements after bipolar cycling as depicted in Fig. S5 of the supplementary. The cycling and measurement amplitudes for MFM devices were 3 V and for MFIM devices 7.5 V to take the voltage drop over the AlO_x and or NbO_x layers into account.

The IV- and PV-curves measured with increasing amount of bipolar cycling of the MFM sample and the MFM samples with a NbO_x layer inserted are shown in Fig. 5.

The device without NbO_x shows strong peak splitting in the initial state, which is reduced with increasing amount of cycling. In the pristine HZO device, some of the domains are polarized in the P_{up} state, marked with 1, and some are in the down state, marked with 2, as shown in Fig. 6 a). Applying a positive pulse to one device and a negative pulse to an adjacent device causes the two types of domains to appear separately in the measured IV curves, as shown in Fig. 6 b). The switching peaks show an imprint in opposite directions, which could be a result of accumulated charges at opposing boundaries of the HZO, depending on the polarization state.

The introduction of NbO_x near the top electrode in the HZO.NbO_x device results in more domains of type 2 (average polarization pointing towards the bottom electrode) in the pristine state. Additionally, only domains of type 2 show an imprint to negative voltages, while domains of type 1 show no imprint as the peak position in Fig. 5 c) indicates.

In the third case, with NbO_x at the bottom interface in the NbO_x.HZO device, almost all domains are polarized in the state 1 in the pristine state (average polarization pointing towards the top electrode) and have the same hysteresis shift to positive voltages caused by the internal electric bias field. As a consequence, no peak splitting is observed in this device. The introduction of the NbO_x layer significantly alters the mean average polarization direction in the pristine state and therefore the initial distribution of domains with an up- or downward projected polarization vector. The opposing average bias shift in the HZO.NbO_x (shift to negative voltages) and NbO_x.HZO (shift to positive voltages) samples shows that the bias shift depends on the position of the NbO_x layer in the stack. The bias shift is

most likely caused by accumulated charges in the NbO_x layer or its neighbouring interfacial regions, which could either emanate from charged trap sites¹⁸ or the presence of charged oxygen vacancies in the HZO. The XPS measurements have shown an increased amount of vacancies in the HZO when it is in direct contact with the NbO_x , but an influence of trap sites can't be excluded.

The influence of the NbO_x layer on the distribution of domain types 1 and 2 is presumably more dominant in the NbO_x .HZO sample than in the HZO. NbO_x sample, because of either a higher chemical interaction between HZO and NbO_x during the ALD process or due to the increased amount of oxygen in the NbO_x layer of the NbO_x .HZO sample as shown in Fig. 3. Furthermore, the formation of alloys between HZO and NbO_x can't be excluded, as it is already shown by P. Luo et al.¹⁹ for ZrO_2 - Ta_2O_5 - Nb_2O_5 systems.

Bipolar cycling removes the accumulated vacancies from the interfaces and redistributes them in the HZO layer,^{4,5,20} which results in the observed reduction of the peak splitting and reduction of the bias shift with cycling.⁴

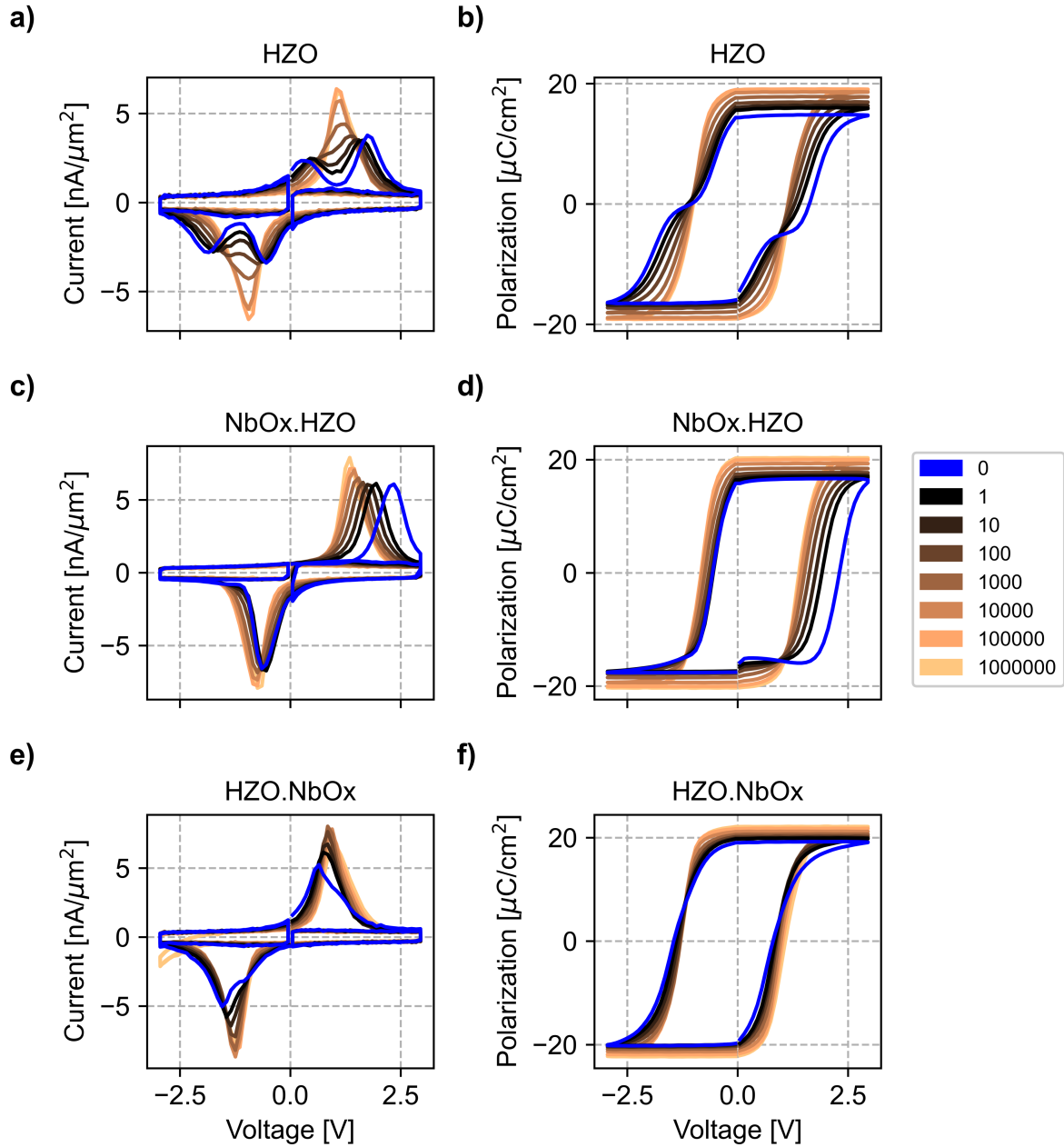


Figure 5: IV- and PV-curves from PUND measurement with increasing cycling number for the investigated HZO sample in a) and b), the $\text{NbO}_x\text{.HZO}$ sample in c) and d) as well as the HZO.NbO_x sample in e) and f). For the IV-curves the current densities vs the applied voltages are plotted and for the PV loops the difference of P-U and N-D pulses is used to estimate the polarization.

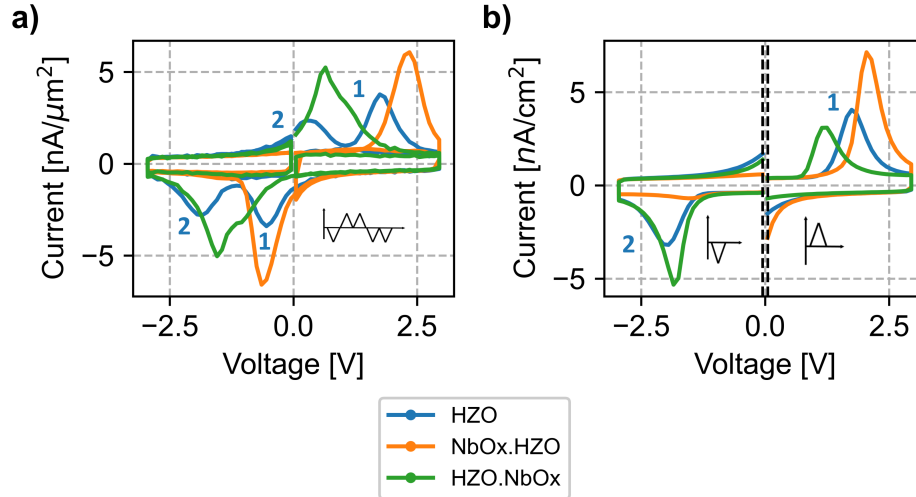


Figure 6: PUND measurements for the pristine devices are shown in a) with the assignment of switching peaks to domain types for the HZO device. Before the PUND measurement a pre-pulse is used to bring the domains in the same state. The IV-curves measured with the application of either a positive or a negative pulse on two distinct pristine devices are shown in b). Blue shows the HZO sample, orange the NbO_x.HZO sample and green the HZO.NbO_x sample.

Electrical analysis of MFIM with NbO_x incorporation

The measured IV-curves and PV-curves of the MFIM sample and of the three MFIM samples with an inserted NbO_x layer are shown in Fig. 7.

All samples exhibit similar behavior except for the HZO.NbO_x.AlO_x one. Peak splitting is observed for positive voltages, but the second peak at a higher voltage (>5 V) can not be fully measured due to the breakdown of the device. Only one peak is observed for negative voltages, which may arise from leakage mediated switching due to charge injection^{21,22} through the AlO_x. The observed peak splitting consistently decreases with cycling, similar to what is observed in the MFM samples. The two switching peaks can be separated into domains of type 1 (P_{up} domains in the pristine state with positive bias shift) and type 2 (P_{down} domains with negative bias shift in the pristine state) as shown in Fig. 8 a) and b). The incorporation of NbO_x below the HZO layer in the NbO_x.HZO.AlO_x device results in a shift of the IV curve to positive voltages, which is consistent with the observed behavior for

the $\text{NbO}_x\text{.HZO}$ device. However, the device still shows peak splitting in the pristine state. The $\text{HZO.AIO}_x\text{.NbO}_x$ sample shows no bias shift of the IV-curve in the pristine state (Fig. 8 (a)) in comparison to the HZO.AIO_x device, because there is no direct contact between the HZO and the NbO_x layer and therefore no additional vacancies are generated in the HZO for this sample. Consequently, the behaviors of HZO.AIO_x and $\text{HZO.AIO}_x\text{.NbO}_x$ in the pristine state are very similar. After bipolar cycling, the devices show a deviation in their behaviour. The device $\text{HZO.NbO}_x\text{.AIO}_x$ shows almost no wakeup, no peak splitting in the pristine state and a very symmetric IV-curves as shown in Fig.7. However, the endurance of the device is reduced to $1e4$ in comparison to $1e5$ cycles for the other MFIM devices with AIO_x layer. The lack of imprint and peak splitting for positive voltages indicates that the switching mechanism for positive voltages is driven by leakage as in the case for negative voltages.

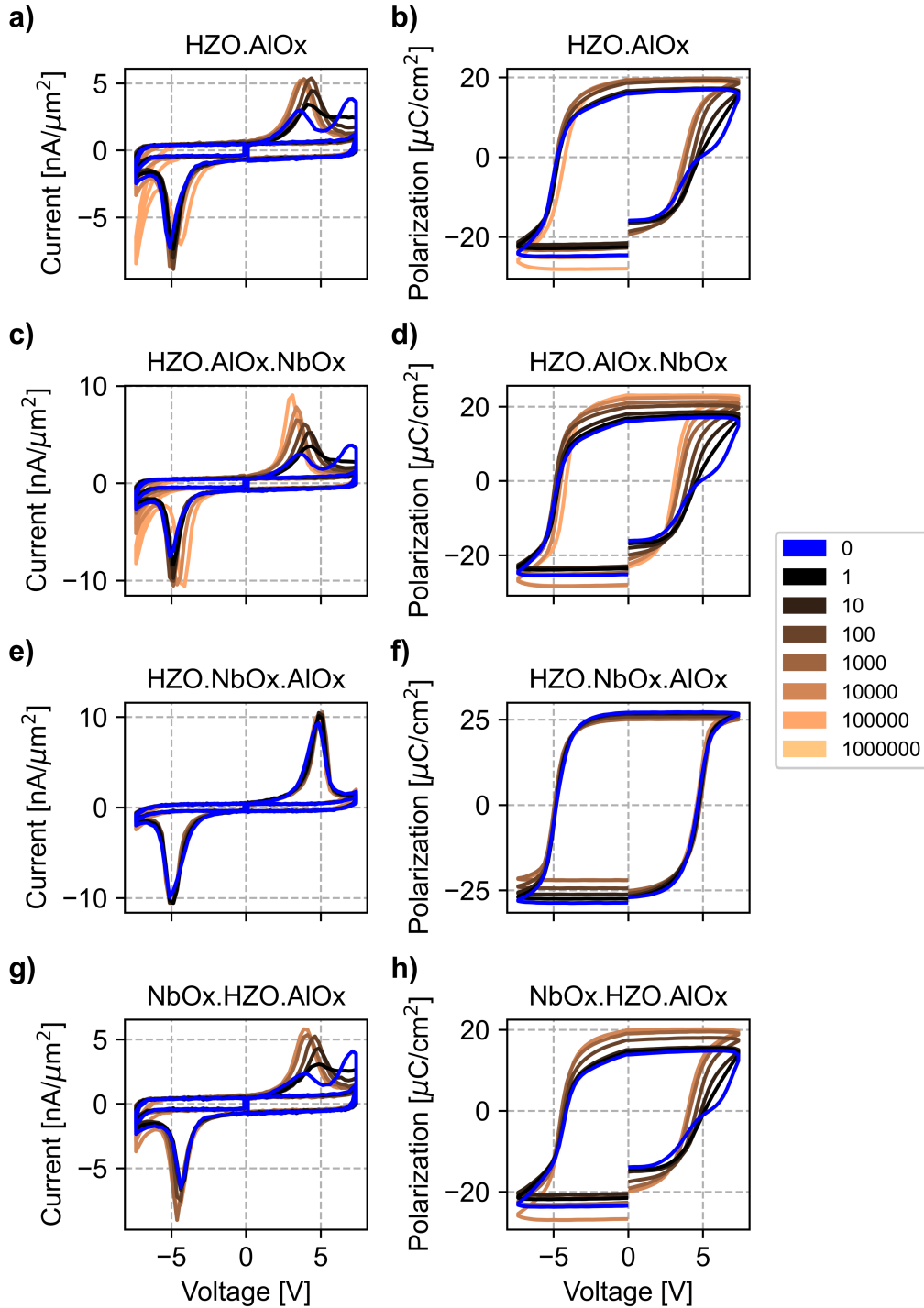


Figure 7: IV- and PV-curves from PUND measurement with increasing cycling number for the investigated HZO.AIO_x sample in a) and b), the HZO.AIO_x.NbO_x sample in c) and d), the HZO.NbO_x.AIO_x sample in e) and f), as well as the NbO_x.HZO.AIO_x sample in g) and h). For the IV-curves the current densities vs the applied voltages are plotted and for the PV loops the difference of P-U and N-D pulses is used to estimate the polarization.

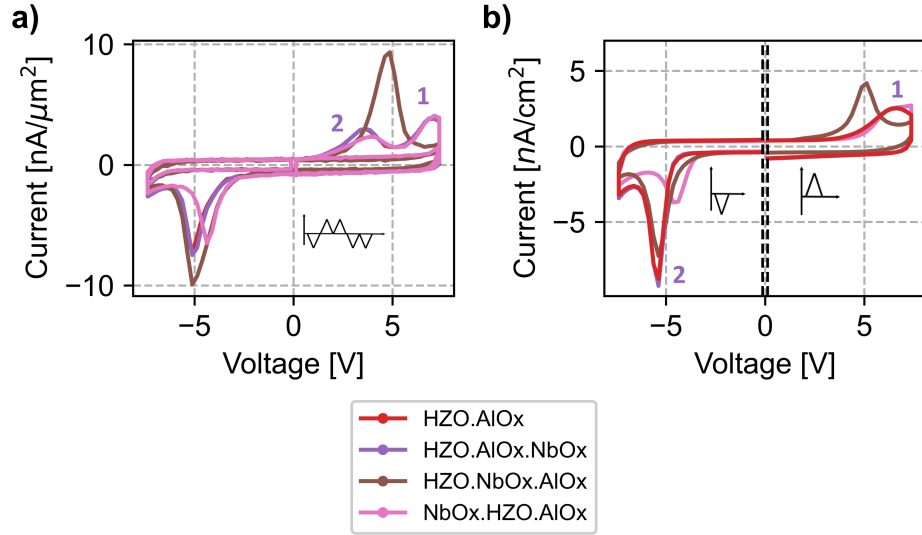


Figure 8: PUND measurements for the pristine devices are shown in a) with the assignment of switching peaks to domain types for the HZO device. Before the PUND measurement a pre-pulse is used to bring the domains in the same state. The IV-curve for the application of a positive and negative pulse at two separate, pristine devices is shown in b). Red shows the HZO.AIO_x, purple the HZO.AIO_x.NbO_x, brown the HZO.NbO_x.AIO_x and pink the NbO_x.HZO.AIO_x

In the study by Si et. al.²¹ a charge trapping induced switching model is used to describe the switching behavior of HZO/AIO_x stacks, which could explain the reduced effect of NbO_x in the NbO_x.HZO.AIO_x device compared to the one in the NbO_x.HZO device. The observed device behavior is consequently not entirely dominated by the generated vacancies of the NbO_x layer, but by charge injection processes over the AIO_x layer.

Assuming a series capacitance of HZO and AIO_x capacitors, with a 4 nm AIO_x and 10 nm HZO thicknesses and a dielectric constant of 30 for the HZO and 7 to 9 for AIO_x, then the switching voltage of the device should be between 2.7 and 3.4 V, assuming a necessary voltage drop of 1.2 V over the HZO layer for switching the domains.

Nevertheless, the observed switching peaks for the HZO.AIO_x device in the cycled state are around ±5 V and is higher than the calculated voltage with the series capacitance model. It can be assumed that the device behavior is strongly influenced by charge traps at the HZO-/AIO_x interface and that the charge injection mechanism plays a crucial role in the device

properties such as switching fields. The asymmetric IV curve of the HZO. AlO_x device could be due to different dominant charge injection mechanism for positive and negative voltages. For the HZO. NbO_x . AlO_x device, the charge injection mechanism is modified by the NbO_x layer, resulting in a symmetric IV curve.

Conclusion

The experiments show that the insertion of a NbO_x layer in MFM devices based on hafnium zirconium oxide modifies the pristine device properties such as imprint and peak-splitting when the NbO_x is in direct contact with the HZO layer. The NbO_x scavenges oxygen from the neighboring HZO layer and creates double positively charged oxygen vacancies in the HZO, which are likely the cause of the observed imprint when NbO_x is introduced into the MFM stack.

A stronger influence of the NbO_x layer is observed in NbO_x .HZO devices compared to HZO. NbO_x ones, which is most likely related to the increased amount of oxygen in the NbO_x layer as shown in EELS measurements and thus the exposure of the NbO_x layer in the NbO_x .HZO sample to the ALD process.

In addition, inserting the NbO_x layer into the stack causes a preferred polarisation state whose direction depends on the position of the NbO_x in the stack. The preferred polarisation state is most likely related to the electric bias field caused by the charged oxygen vacancies at the HZO-/ NbO_x interface. The influence of the introduced NbO_x layer causes similar bias shifts in the pristine device state as previously reported for the incorporation of thin tantalum oxide layer^{3,16} in HZO-based MFM capacitors. Unlike MFM stacks with a tantalum oxide layer, where the bias shift is caused by the creation of fixed charges in the tantalum oxide, the bias shift in our devices reduces with cycling, which is most likely caused by a redistribution of vacancies in the HZO layer.^{4,5}

The introduction of a NbO_x layer in MFIM stacks based on a stack of HZO and AlO_x shows

the expected bias shift in the $\text{NbO}_x\text{.HZO.AIO}_x$ sample, but the influence is not as strong as in the $\text{NbO}_x\text{.HZO}$ sample. A possible explanation is the influence of charge trapping induced switching at the HZO-AIO_x interface. The switching process is then at least partially defined by the charge trapping process, which can explain the asymmetric device behavior and the deviation of the measured switching voltages and the switching voltages extracted from a series capacitance model. The incorporation of NbO_x in between HZO and AlO_x in the $\text{HZO.NbO}_x\text{.AlO}_x$ device leads to a symmetric IV curve. A likely cause is the change of the AlO_x layer by the adjacent NbO_x layer. Further experiments are necessary to identify the charge injection mechanism and its modification by the incorporation of NbO_x in the $\text{HZO.NbO}_x\text{.AlO}_x$ device.

Acknowledgement

M.E. acknowledges funding from the German Research Foundation as part of the FeDiBiS project with project ID 449644906.

C.D., S.S. acknowledge funding from the European Union's Horizon research and innovation programme under grant agreement 101135398 (FIXIT).

L.C. acknowledges funding from the European Union's European Innovation Council under Grant Agreement No. 101070908 (CROSSBRAIN).

S.L. acknowledges funding from European Union's Horizon research and innovation programme (Grant agreement No. 101135656) Ferro4EdgeAI

C.D. and I.H. acknowledge funding by the European Union of the project number 101098216 (ERC Advanced Grant, LUCIOLE,). Views and opinions expressed are, however, those of the authors only and do not necessarily reflect those of the European Union or the European Research Council Executive Agency. Neither the European Union nor the granting authority can be held responsible for them.

T.M. acknowledges funding from the Saxonian State budget approved by the delegates of the Saxon State Parliament.

Supporting Information Available

The supplementary information contains additional information about electric, EELS and XPS measurements.

A description of how to generate the cross section shown in Fig. 2 is given.

Furthermore, XPS measurements on the Hf 3d core level of the device HZO.NbO_x.AlO_x as well as XPS measurements on the Al 2p core level for the devices HZO.AlO_x and HZO.NbO_x.AlO_x are shown.

The electrical measurement setup, the electrical parameters of the samples used in XPS, and the P_r development of the investigated MFM and MFIM samples with increasing bipolar cycling are shown.

In addition, the IV development with cycling for different voltages of the HZO.NbO_x.AlO_x device is shown.

References

- (1) Kim, S. J.; Mohan, J.; Summerfelt, S. R.; Kim, J. Ferroelectric Hf 0.5 Zr 0.5 O 2 thin films: A review of recent advances. *Jom* **2019**, *71*, 246–255.
- (2) Scott, J. F.; Kammerdiner, L.; Parris, M.; Traynor, S.; Ottenbacher, V.; Shawabkeh, A.; Oliver, W. F. Switching kinetics of lead zirconate titanate submicron thin-film memories. *Journal of Applied Physics* **1988**, *64*, 787–792.
- (3) Jeong, Y.; Gaddam, V.; Goh, Y.; Shin, H.; Lee, S.; Kim, G.; Jeon, S. Oxygen vacancy control as a strategy to enhance imprinting effect in Hafnia ferroelectric devices. *IEEE Transactions on Electron Devices* **2022**, *70*, 354–359.
- (4) Lee, S.; Ronchi, N.; Bizindavyi, J.; Popovici, M. I.; Banerjee, K.; Walke, A.; Delhougne, R.; Van Houdt, J.; Shin, C. Analysis of wake-up reversal behavior induced by imprint in La: HZO MFM capacitors. *IEEE Transactions on Electron Devices* **2023**, *70*, 2568–2574.
- (5) Pešić, M.; Fengler, F. P. G.; Larcher, L.; Padovani, A.; Schenk, T.; Grimley, E. D.; Sang, X.; LeBeau, J. M.; Slesazek, S.; Schroeder, U.; Mikolajick, T. Physical Mechanisms behind the Field-Cycling Behavior of HfO₂-Based Ferroelectric Capacitors. *Advanced Functional Materials* **2016**, *26*, 4601–4612.
- (6) Walke, A. M.; Popovici, M. I.; Sharifi, S. H.; Demir, E. C.; Puliyalil, H.; Bizindavyi, J.; Yasin, F.; Clima, S.; Fantini, A.; Belmonte, A.; others La Doped HZO based 3D-Trench Metal-Ferroelectric-Metal Capacitors with High Endurance (> 10¹²) for FeRAM Applications. *IEEE Electron Device Letters* **2024**,
- (7) Popovici, M.; Bizindavyi, J.; Favia, P.; Clima, S.; Alam, M. N. K.; Ramachandran, R.; Walke, A.; Celano, U.; Leonhardt, A.; Mukherjee, S.; others High performance La-doped HZO based ferroelectric capacitors by interfacial engineering. 2022 International Electron Devices Meeting (IEDM). 2022; pp 6–4.

- (8) Nandi, S. K.; Liu, X.; Li, S.; Venkatachalam, D. K.; Belay, K.; Elliman, R. G. Resistive switching behavior in HfO₂ with Nb as an oxygen exchange layer. 2014 Conference on Optoelectronic and Microelectronic Materials & Devices. 2014; pp 290–293.
- (9) Engl, M.; Mikolajick, T.; Slesazeck, S. Degradation of Nonhysteretic Switching in HZO–Al₂O₃ Stacks Due to Positive Unipolar Stress. *IEEE Transactions on Electron Devices* **2023**,
- (10) Lancaster, S.; Arnay, I.; Guerrero, R.; Gudín, A.; Guedeja-Marrón, A.; Diez, J. M.; Gärtner, J.; Anadón, A.; Varela, M.; Camarero, J.; Mikolajick, T.; Perna, P.; Slesazeck, S. Toward Nonvolatile Spin–Orbit Devices: Deposition of Ferroelectric Hafnia on Monolayer Graphene/Co/HM Stacks. *ACS Applied Materials & Interfaces* **2023**, *15*, 16963–16974.
- (11) Alcalá, R.; Materano, M.; Lomenzo, P. D.; Vishnumurthy, P.; Hamouda, W.; Dubourdieu, C.; Kersch, A.; Barrett, N.; Mikolajick, T.; Schroeder, U. The Electrode–Ferroelectric Interface as the Primary Constraint on Endurance and Retention in HZO–Based Ferroelectric Capacitors. *Advanced Functional Materials* **2023**, *33*, 2303261.
- (12) Lee, Y.; Goh, Y.; Hwang, J.; Das, D.; Jeon, S. The influence of top and bottom metal electrodes on ferroelectricity of hafnia. *IEEE Transactions on Electron Devices* **2021**, *68*, 523–528.
- (13) Hsain, H. A.; Lee, Y.; Lancaster, S.; Materano, M.; Alcalá, R.; Xu, B.; Mikolajick, T.; Schroeder, U.; Parsons, G. N.; Jones, J. L. Role of Oxygen Source on Buried Interfaces in Atomic-Layer-Deposited Ferroelectric Hafnia–Zirconia Thin Films. *ACS Applied Materials & Interfaces* **2022**, *14*, 42232–42244.
- (14) Hamouda, W.; Pancotti, A.; Lubin, C.; Tortech, L.; Richter, C.; Mikolajick, T.; Schroeder, U.; Barrett, N. Physical chemistry of the TiN/HfO₂. 5ZrO₂ interface. *Journal of Applied Physics* **2020**, *127*.

- (15) Hamouda, W.; Mehmood, F.; Mikolajick, T.; Schroeder, U.; Mentès, T. O.; Locatelli, A.; Barrett, N. Oxygen vacancy concentration as a function of cycling and polarization state in TiN/Hf_{0.5}Zr_{0.5}O₂/TiN ferroelectric capacitors studied by x-ray photoemission electron microscopy. *Applied Physics Letters* **2022**, *120*.
- (16) Shin, H.; Gaddam, V.; Goh, Y.; Jeong, Y.; Kim, G.; Qin, Y.; Jeon, S. A method of controlling the imprint effect in hafnia ferroelectric device. *Applied Physics Letters* **2023**, *122*.
- (17) Jacob, K.; Shekhar, C.; Vinay, M.; Waseda, Y. Thermodynamic properties of niobium oxides. *Journal of Chemical & Engineering Data* **2010**, *55*, 4854–4863.
- (18) Zhang, L.; Raza, M. H.; Wu, R.; Gruel, K.; Dubourdieu, C.; Hÿtch, M.; Gatel, C. Quantification of Interfacial Charges in Multilayered Nanocapacitors by Operando Electron Holography. *Advanced Materials* **2024**, 2413691.
- (19) Luo, P.; Wu, X.; Xiao, W.; Zhang, F.; Wang, Y.; Huang, D.; Du, Y. Phase equilibria in the ZrO₂–Ta₂O₅–Nb₂O₅ system: experimental studies and thermodynamic modeling. *Journal of the American Ceramic Society* **2022**, *105*, 668–686.
- (20) Starschich, S.; Menzel, S.; Böttger, U. Evidence for oxygen vacancies movement during wake-up in ferroelectric hafnium oxide. *Applied Physics Letters* **2016**, *108*.
- (21) Si, M.; Lyu, X.; Ye, P. D. Ferroelectric polarization switching of hafnium zirconium oxide in a ferroelectric/dielectric stack. *ACS Applied Electronic Materials* **2019**, *1*, 745–751.
- (22) Fontanini, R.; Barbot, J.; Segatto, M.; Lancaster, S.; Duong, Q.; Driussi, F.; Grenouillet, L.; Triozon, L.; Coignus, J.; Mikolajick, T.; others Interplay between charge trapping and polarization switching in beol-compatible bilayer ferroelectric tunnel junctions. *IEEE Journal of the Electron Devices Society* **2022**, *10*, 593–599.